

# Manipulation Planning for the Atlas Humanoid Robot

Cong Du, Wyatt Newman, *Senior Member, IEEE*

**Abstract**—Kinematic planning for performing manipulation tasks with an Atlas humanoid robot is presented. A hybrid analytic/numerical inverse kinematics approach is described, yielding fast solutions. The solution technique supports extensive exploration of manipulation strategies. Task-specific optimization metrics are introduced, leading to manipulation plans for three tasks: acquiring a horizontal cylinder, turning a valve, and turning a door handle.

## I. INTRODUCTION

TEAM HKU, based at University of Hong Kong, is competing in the DARPA Robotics Challenge (DRC). DARPA challenge tasks are detailed in [1]. This competition is based on a disaster-response scenario, and many of the tasks require mobile manipulation, including grasping and using power tools, driving a vehicle, turning valves and opening doors.

Team HKU is using an “Atlas” humanoid robot from Boston Dynamics [2] equipped with Sandia hands [3]. Although Atlas’s arms each have 6 degrees of freedom, finding viable trajectories for manipulation tasks has been more difficult than anticipated. The kinematic structure and the joint limits of the arms highly constrain the manipulability. Further, the arm design does not offer an analytic inverse kinematic solution.

Our approach to addressing these limitations is described here, illustrated in three manipulation tasks: grasping a horizontal cylinder, turning a valve, and turning a door handle.

## II. HYBRID INVERSE KINEMATICS METHOD FOR ATLAS

When an analytic inverse kinematic solution is not available, one conventionally resorts to numerical inverse kinematics. Although progress has been made in developing general-purpose inverse kinematics solvers, such as [4], numerical inverse kinematics solvers still suffer from multiple limitations. These include: inability to identify all alternative solutions; unexpected switching between alternative solutions during a desired smooth trajectory; numerical instability; convergence to local minima; potentially long computation times; and potential inability to recognize that a solution does not exist.

Cong Du is a Master’s student at Hong Kong University (ducong@hku.hk).

Wyatt Newman, EECS Dept, Case Western Reserve University, Cleveland, OH, is currently the Hung Hing Ying Distinguished Visiting Professor in Science and Engineering at HKU (e-mail: wyatt.newman@case.edu)

In contrast, an analytic solution yields the entire set of solutions and never has instability or convergence problems.

Although Atlas’s arms do not offer an analytic solution, we can derive most of the benefits of an analytic solution using an approximate approach, augmented with numerical iterations.

### A. Modeling Atlas with Denavit-Hartenberg parameters

A partial schematic figure of Atlas’s kinematics is shown in Fig 1:

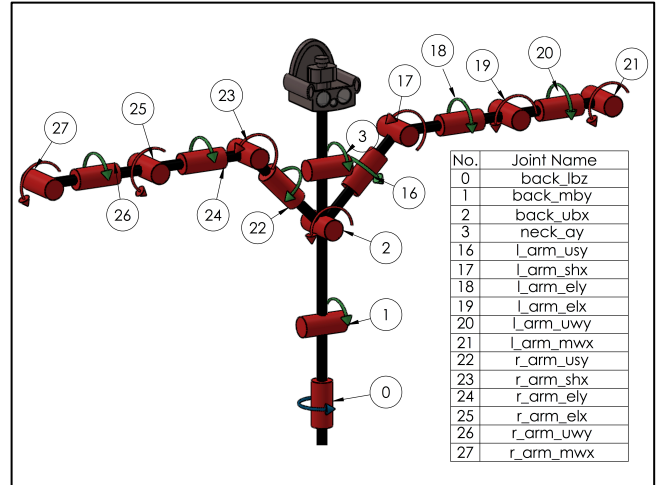


Fig. 1. Schematic of Atlas’s upper body kinematics

Table I summarizes the right arm kinematics of Atlas in terms of Denavit-Hartenberg [5] parameters. The first row is a static transformation from a convenient reference frame in the torso to the first arm joint. From Fig 1, it is noteworthy that the arms do not include a tool-flange rotation capability. This omission is largely responsible for severe manipulability limitations.

TABLE I DENAVIT HARTENBERG PARAMETERS FOR RIGHT ARM

Frame transform	<i>d</i>	<i>a</i>	$\alpha$	$\theta$
Torso to usy	0.079	0.052	$7\pi/6$	0
Usy to shx	-0.5172	0.0235	$\pi/2$	q1
Shx to ely	0	0.016	$\pi/2$	q2
Ely to elx	-0.306	0.0092	$-\pi/2$	q3
Elx to uwy	0	0.0092	$-\pi/2$	q4
Uwy to mwx	-0.306	0.0092	$-\pi/2$	q5
Mwx to flange	0	0	$\pi/2$	q6

In Table I, the final frame is arbitrarily chosen to have its origin coincident with the next to last frame (thus defining zero *a* and *d* parameters) and to have its z axis point through the center of the tool flange. An additional static transform

relates this final Denavit-Hartenberg frame to a convenient manipulation frame associated with an end effector.

### B. Building hybrid inverse kinematics for Atlas

A significant, early theoretical success in inverse kinematics was the recognition that a 6-DOF robot arm with a spherical wrist always yields an analytic inverse-kinematic solution [7]. The proof is by construction, using the definition of a “wrist point” at the intersection of the last 3 joint axes. When a wrist point exists, the required 3-D coordinates of this point follow from a specification of the desired hand frame. Since the wrist point location is only a function of the first 3 proximal joints, for a 6-DOF arm, this leads to a (nonlinear) system of three equations in 3 unknowns. With this sub-system simplification, all variations of kinematic configurations of 3 joints have been analyzed to show that this simpler problem can be solved, and subsequently the 3 wrist degrees of freedom follow as well.

Unfortunately, Atlas does not have a spherical wrist. In fact, the construction has no intersecting joints; all successive joint axes have non-zero offsets ( $a$ -parameters), which complicates performing inverse kinematics.

Rather than resort to numerical solutions, a custom approximate analytic inverse kinematics solution was developed. This is achieved by ignoring the two shoulder offsets, thus approximately modeling the arms as having spherical shoulders. This approximation allows the definition of a “shoulder” point, S, at the intersection of the first 3 joint axes. Although there is no spherical wrist, we define a “wrist point”, W, at the origin of the final D-H frame (which lies on the wrist-bend axis). In addition, we define an “elbow point”, E. The elbow point is the origin of the elx frame (the frame defined on the elbow-bend axis, ignoring offset  $a_3$ ). Subject to the above approximation, the elbow point 3-D coordinates must satisfy two separate constraints: one in terms of the first two joints, and the other in terms of the last (wrist-bend) joint.

Following the logic of [6,7,8], from specification of the desired hand frame, one can compute the corresponding location of the “wrist point” W. Additionally, the direction of the last joint axis (wrist bend) follows from the hand frame constraint. Consequently, the elbow point must lie on a circular arc about the wrist-bend axis, in a plane perpendicular to this axis. The radius of this arc is equal to the forearm length ( $d_4+d_6$  in Table I).

The second constraint on the elbow-point location follows from the spherical-shoulder approximation. The elbow point must lie on a sphere about the shoulder point, with radius equal to the length of the humerus ( $d_2$  in Table I). The location of the elbow point on this sphere is a function only of joints 1 and 2.

Coordinates of the elbow point follow from the intersections between the circular-arc constraint and the spherical constraint, as illustrated in Fig 2. These intersections can be found analytically, yielding 0, 1 or 2 solutions. (Details of solving this geometric problem are straightforward and are omitted here). The joint angles for  $q_1$ ,  $q_2$  and  $q_6$  follow. Analogous to the method of [8], the

remaining joint angles follow analytically from this partial solution.

The analytic constraints yield solutions, including identifying any/all alternatives. In the absence of joint limits and self-collision considerations, poses that are within the reach of the approximate kinematic model (and away from singularities) theoretically have 8 inverse-kinematic solutions. However, once Atlas’ joint limits are imposed, occurrences of multiple solutions are rare. Based on the approximate model, there are provably at most 2 reachable inverse-kinematic solutions. In extensive random testing, these occurred only 30% of the time. Roughly speaking, if an inverse kinematic solution exists, the solution is most often unique within joint-limit constraints.

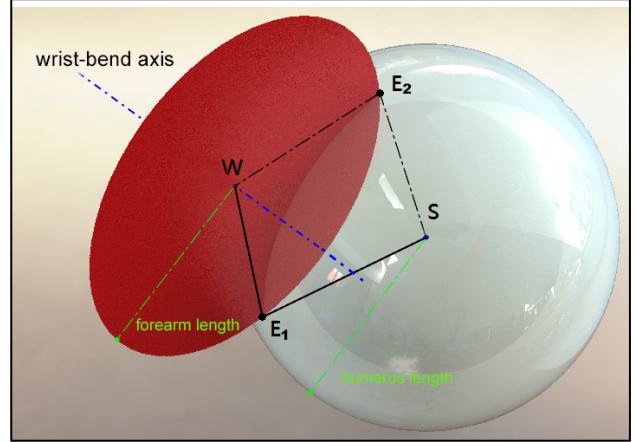


Fig. 2. Illustration of spherical and circular-arc constraints. For a spherical shoulder joint, the shoulder point, S, and the wrist point, W, constrain the elbow point to lie at the intersections of a circular arc and a sphere, E1 or E2.

The solutions obtained analytically--based on a spherical-shoulder approximation--yield exact matches to the target hand orientations, but the hand positions are in error. From tests, the analytic solutions differed from exact solutions on average by approximately 1.8cm. Using the approximate, analytic solutions as seed values for numerical solutions, precision solutions can be found quickly, typically converging within round-off error within 3 iterations.

The existence of this fast and exhaustive technique for finding inverse-kinematics solutions enables exploration of manipulation strategies.

### C. Kinematics implementation in ROS

Inverse kinematics for Atlas’ arms has been implemented by TeamHKU within a library compatible for use within Robot Operating System (ROS [9]) nodes. The implementation utilizes the open-source ROS package “Kinematics and Dynamics Library”, KDL [10]. The implementation also uses the ROS-compatible Eigen library [11]. On one core of a 3.4GHz Intel i7 processor, the inverse-kinematics implementation computes solutions at 20kHz, making it practical to perform extensive searches for manipulation planning.

### III. MANIPULATION PLANNING

To plan manipulations, we define a reference grasp frame on the end effector. A photo of the palm of the Sandia hand and our defined palm frame appears in Figure 3.

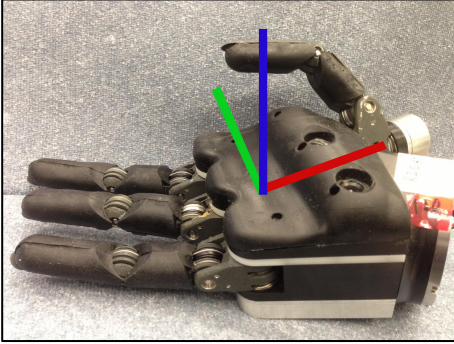


Fig. 3. Sandia hand showing palm cameras and palm shape with defined grasp frame on hand palm. Palm normal is blue, and green y-axis is parallel to the raised (hump) feature.

With respect to this defined palm frame, one can analyze some useful categories of grasps. For example, to grab a cylindrical object sitting upright on a table (e.g., a water bottle), one would want to position the hand with the y-axis (the green palm-frame axis) oriented vertically. Another useful category is grasp of cylinders lying on the side, such as a hammer lying on a table. For this type of grasp, one would want to approach the object from above, corresponding to the palm normal pointing downwards. Additionally, one would want to align the palm-frame y-axis with the cylindrical object's axis. For wheel or valve turning using the palm, the palm normal (the blue axis) should be oriented radially inwards, pointing towards the wheel's axis. Manipulation planning for three representative tasks is presented next.

#### A. Horizontal grasp evaluation

Visualizing manipulability in 6 degrees of freedom of task space is difficult. A variety of approaches has been taken. In [12], reachability is illustrated by displaying colorized points in 3-D, where the point location corresponds to the end-effector position and the color corresponds to the number of orientations reachable at that position.

Such plots are useful for visualizing regions of space that are impossible to reach at any orientation. However, the operator needs additional information to visualize what is possible to reach—including visualization of achievable grasp orientation. Oriented Reachability Maps are described in [13], for which templates are precomputed to visualize candidate platform locations to achieve a specific grasp pose. These templates are colorized to indicate manipulability, including consideration of joint limits and Jacobian sensitivities. Here, we take a related approach, but specialize on consideration of grasp approach for specific task categories.

One useful manipulation capability is to grasp a horizontal cylinder. The style of grasp considered may be categorized as a cylindrical power grasp (specifically: power->

prehensile->prismatic->heavy wrap->small diameter [14]). Commonly, the cylinder to be grasped may be lying on a flat surface, for which approach should be from above. The grasp pose specification is thus defined in terms of the hand's grasp-frame origin with the constraint that the palm normal points down.

Reachable poses of this type were analyzed using our fast inverse-kinematics solver. With specified grasp-frame origin and direction of palm normal, there is one unspecified degree of freedom: the direction of the grasp-frame y-axis in the horizontal plane. The green vectors shown in Fig 4 are gripper-frame y-axes, emanating from sampled grasp-frame origins. Each bundle of vectors illustrates the range of options for palm rotation about palm normal for which right-hand inverse kinematic solutions exist within the joint limits. This figure also illustrates how highly constrained the options are for inverse-kinematic solutions.

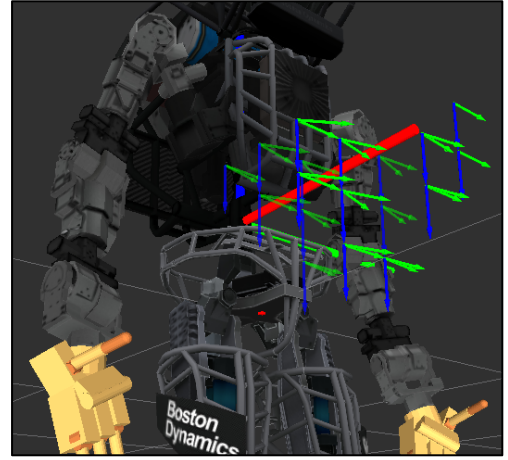


Fig. 4. Reachable power grasps with palm normal down. Green vectors indicate viable y-axis directions of the palm grasp frame.

Beyond a pose being reachable, there are additional considerations for a desirable grasp approach. Solutions that are too close to a joint limit should be avoided, since fine-motion corrections would be constrained. Another consideration is Jacobian singularities (or near singularities). Pose solutions that result in nearly-singular Jacobians should be avoided, since fine-motion corrections about these poses may require large joint-angle changes. Additionally, when approximate analytic solutions are used to seed numerical solutions, convergence is rapid, except when the Jacobian is nearly singular. For both of these reasons, poses near singularities should be avoided.

To evaluate the meaning of “near” singularities, inverse-kinematics solutions were analyzed in terms of numerical convergence rates. It was observed that columns of the Jacobian-inverse could be evaluated to predict whether a numerical solution could be obtained easily—and this also indicated poses for which fine manipulation adjustments could be performed readily. For the Denavit-Hartenberg parameters of this system, a pose was considered “manipulable” if the magnitude of all elements of the first three columns of the Jacobian inverse were less than 6m/rad

and those of the last three columns were less than 2m/rad. A manipulability index was defined as:

$$\tau \leftarrow \begin{cases} \text{true: } & \max|J_{i,j}^{-1}| \leq 6 \ (i \in \{1, \dots, 6\}, j \in \{1, 2, 3\}) \\ & \max|J_{i,j}^{-1}| \leq 2 \ (i \in \{1, \dots, 6\}, j \in \{4, 5, 6\}) \\ \text{false: } & \text{otherwise} \end{cases}$$

When a pose was thus determined to be “manipulable”, numerical iterations from the approximate solution converged to less than 1-micron error and less than 1m/rad error within only 3 iterations. Hand poses for which this was true allowed for fine-motion corrections in all 6 dimensions. Such poses were identified as the most attractive for attempting manipulation.

Another view of horizontal cylindrical grasp options is shown in Fig 5. This top-down view corresponds to graspability in a horizontal plane 20cm above the pelvis frame (roughly, a common table height). The bundles of green vectors show the ranges of reachable grasps, illustrated as viable grasp-frame y-axis directions. Black vectors indicate “manipulable” poses. Additionally, red colored markers indicate “approachable” poses. A pose is considered “approachable” if the target pose can be reached by pure descent from 20cm above with fixed orientation. Approachable poses are attractive for collision-free grasp.

Overall, the kinematic search revealed a “sweet spot” for attempting right-handed, vertical-approach grasps, located at roughly 30cm in front of and 20 cm to the right of Atlas’s pelvis origin. This preferred grasp region is constrained to a narrow range of object orientations.

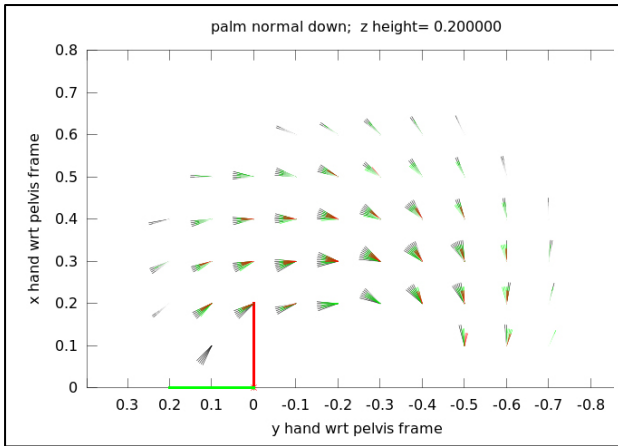


Fig. 5. Illustration of reachable cylindrical grasps with palm normal pointing down, grasp height 20cm above pelvis frame. Vectors are viable orientations of the hand y axis. Black vectors are manipulable poses. Red vectors are approachable poses.

For an object located randomly, it is almost always impossible to achieve the corresponding desired grasp pose within the robot’s joint limits. Instead, grasp tasks must be pre-planned, such that the robot approaches the object to assure that the desired grasp pose is within the robot’s manipulability sweet spot. This kinematic analysis thus provides input to locomotion planning, such that an object to be acquired may be approached in a manner to make grasp feasible.

## B. Motion planning for valve turning

In the context of the task of valve turning, a human would typically perform the task by grasping the rim of the valve wheel and rotating the wheel without grasp slip. The resulting trajectory of 6-DOF hand poses required to turn the valve in this fashion is fully defined in terms of the valve center coordinates, the valve axis direction, and the valve radius. For Atlas’s arms, however, performing no-slip manipulation is infeasible. Rotation of the valve starting from an initial grasp pose, and subject to no-slip between gripper and valve, is only possible for very small valve rotations. Thus, this approach would require regrasping the valve a large number of times after each incremental valve rotation, which is impractically slow.

To achieve practical valve turning, the no-slip grasp constraint may be relaxed. Instead, the valve wheel may be manipulated using the palms only (non-prehensile manipulation). Desirably, if two hands are positioned on the valve wheel diametrically opposed, and if both hands exert a radially inwards force on the valve rim, and if the palm origins are commanded to sweep through a circular arc, then friction between the valve and the palms can be employed to produce the necessary torque to turn the valve wheel. In this approach, it is desirable to keep the palm normals pointed radially inwards, although the hand orientations may rotate about the palm normals during valve rotation. The manipulation task then constrains 5 degrees of freedom of the hand poses, leaving one degree of freedom of null space to exploit.

Using palmar manipulation, inverse kinematic solutions are achievable for long trajectories (large angles of valve turning). In fact, over much of the turning motion, there are multiple (a range of) viable inverse kinematic solutions, similar to the analysis of Figs 4 and 5, allowing for optimization of other considerations.

An optimization condition that we considered was how best to use compliant-motion control implemented on a subset of joints (the humerus joints only). For high-speed valve turning, we had competing considerations of achieving good tracking of the nominal circular trajectory while simultaneously exerting radial forces on the valve wheel. Generally, position control is better for good tracking, and force control (we use Natural Admittance Control [15]) is better for compliant interaction. We chose to control the upper arm (humerus joint) under NAC and the remaining joints under stiff position control. This partitioning, however, required that the robot’s arm poses be planned such that compliance of the humerus would be sufficient to achieve the desired radial forces.

To evaluate this condition, we evaluate the Jacobian to define a dimensionless torque sensitivity parameter  $s$  as follows:

$$s \equiv \left( \hat{r} \cdot \frac{\partial p_{hand}}{\partial q_{humerus}} \right) / L_{forearm}$$

where  $\hat{r}$  is a unit vector in the radial direction from the valve

center to the palm contact on the valve rim;  $p_{\text{hand}}$  is the position of the hand's contact point on the valve rim;  $q_{\text{humerus}}$  is the angle of the humerus joint (i.e.,  $q_3$  in Table I); and  $L_{\text{forearm}}$  is the length of the forearm, from the elbow to  $p_{\text{hand}}$ .

The maximum value of  $s$  is unity, which occurs when an incremental motion of the humerus angle produces the maximum possible radial motion of the hand in the direction  $\hat{r}$ . Equivalently (by the duality of effort and flow for the manipulator Jacobian), for  $s$  near unity, a unit radial force on the hand produces the maximum possible torque on the humerus joint. It is desirable to design arm poses for the valve-turning trajectory that maximize  $s$  in order for compliance in the humerus to be effective in exerting radial forces on the valve wheel.

Figure 6 illustrates our optimization results for valve-turning motion planning. The large circle is the circumference of the valve wheel. The “ $\times$ ” markers correspond to approximate analytic inverse kinematic solutions, illustrating the approximation errors relative to the desired circular hand motion. The “+” markers are the precise solutions, obtained from numerical iterations seeded with the approximate solutions. These colored circles are partially filled to visualize the  $s$  sensitivity values. A circle fully filled corresponds to maximum sensitivity, which is desirable, and less filling indicates lower sensitivity. It is also desired that the hand motion about the circle should be able to sweep out a large angle. Large circular motions result in fewer required re-grasps and thus faster valve turning.

This analysis was repeated to optimize over parameters of approach distance and valve height. (The robot could squat to elevate the valve axis relative to the pelvis, if desired). As with the horizontal-grasp analysis, a sweet spot was found. Atlas should approach the valve at a distance of approximately 0.6m from the pelvis frame to the valve, the valve axis should be centered laterally, oriented parallel to the pelvis x axis (i.e. pointing normal to the chest), and it should typically be as high as practical (i.e., the robot should squat as low as practical).

The results illustrated in Fig 6 highlight the best inverse-kinematic solutions for sample poses along the valve-turning trajectory, defined in terms of optimizing with respect to large rotation angles and good kinematic sensitivity metric. However, these poses were computed without consideration of blending them into a continuous trajectory. Consequently, interpolation between these solutions in joint space resulted in large accelerations that limited the valve-turning speed. To create smoother profiles, the joint-space solutions were smoothed using cubic spline approximations [16]. Since the humerus joints were compliantly controlled to produce a radial squeeze, these joints could accommodate kinematic solution imprecision, making joint-space smoothing feasible.

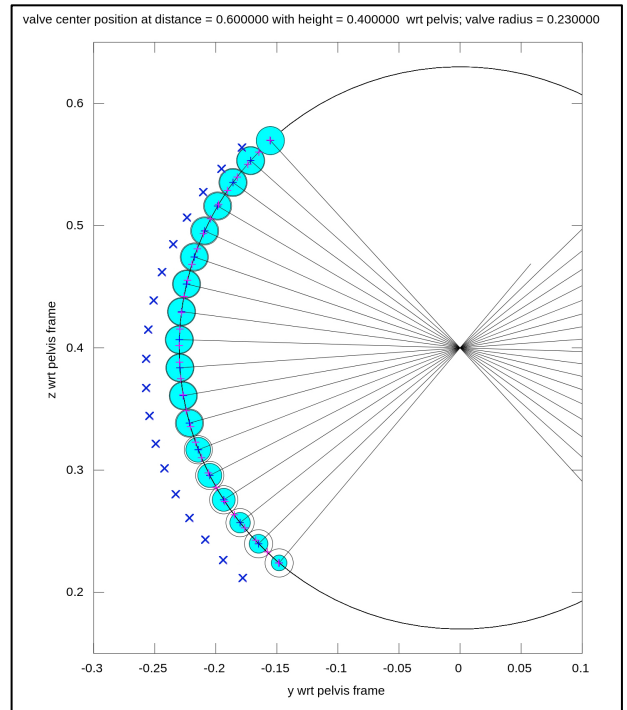


Fig. 6. Trajectory optimization for valve turning. The  $\times$ 's correspond to approximate analytic IK solutions; +'s correspond to accurate IK solutions for circular hand motion with palm normal pointing radially inwards. Colored filling of each circle is proportional to humerus compliance sensitivity at that pose.

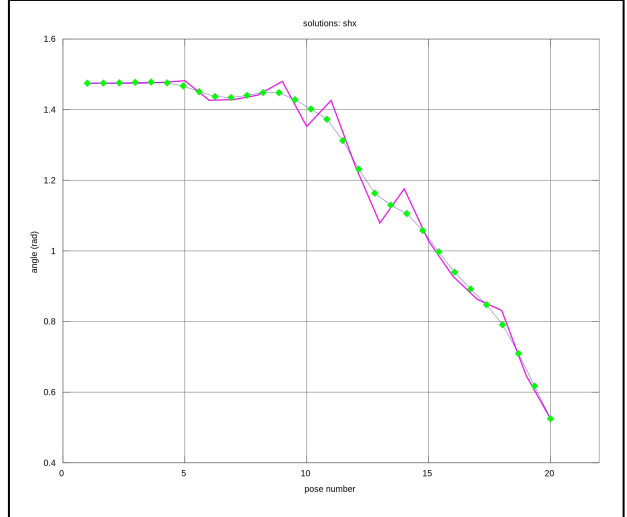


Fig. 7. Result of cubic-spline joint-space smoothing

Figure 7 illustrates smoothing of the trajectory of the shx joint ( $q_2$ ). The original solution (magenta polyline) had saw-tooth features, which resulted in excessive arm accelerations. The smoothed cubic-spline approximation (green curve) was found to be a satisfactory approximation, allowing smooth valve-turning dynamics. For this example, the highest speed achieved was 360-degree rotation of an 18" diameter wheel within 10 seconds.

### C. Motion planning for door handle manipulation

Another DRC task to be performed is to open a door and

pass through it. Approach planning for door-handle manipulation is constrained, in that the robot should be pre-positioned to prepare to side-step through the door once the door is open. Subject to this whole-body placement constraint, there is no kinematically feasible solution for the robot to grasp and manipulate the door handle without slip. In this task, however, the door handle is a lever type, not a round knob, so no-slip grasp is not necessary. The handle may be manipulated by pushing without grasping (e.g., with a closed fist). During this manipulation, the hand may traverse a circular trajectory close to and parallel to the door, but the robot's arm may not hit the door (e.g. with its elbow). Such a trajectory may be enforced by constraining the hand motion to follow the desired arc with the palm normal pointing away from the door. Solutions of this type also have a single degree of freedom of null space, again constrained to rotations about the palm normal. Similar to the horizontal-grasp and the valve-turning analyses, the door-handle manipulation trajectory may be optimized by solving for the range of solutions that satisfy the 5-DOF constraints. Figure 8 illustrates these solutions. The green vectors are the viable directions of the palm-frame y axis for various sample poses along the desired circular hand trajectory. Since door-handle manipulation by pushing does not require precision nor compliant-motion control, optimization of the trajectory is based only on smoothness of the path in joint space.

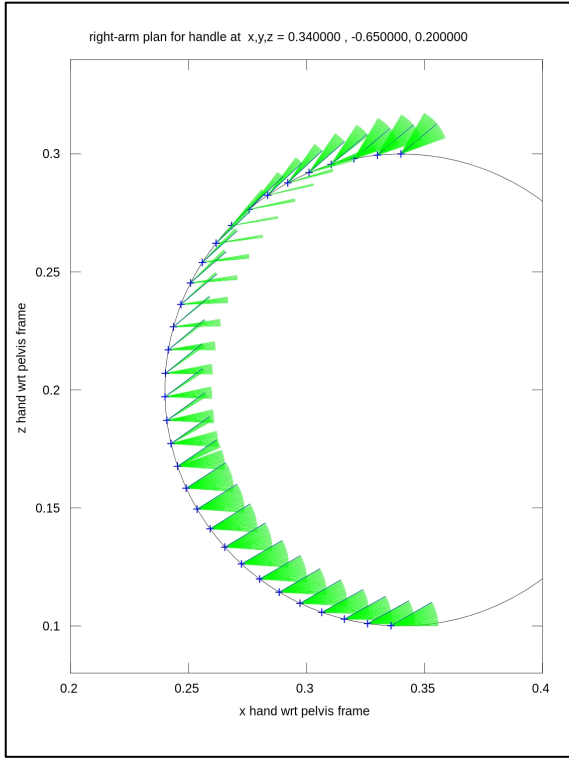


Fig. 8. Valid IK solutions for door handle manipulation task. Green vectors are palm y-axis options for sample points along the circular hand trajectory.

#### IV. CONCLUSION

Analysis of manipulation tasks for “Atlas” is complicated

by the non-existence of an analytic inverse-kinematics solution, as well as by the severe limitations of the kinematic structure and joint constraints. The inverse-kinematics problem has been addressed using an analytical solution that invokes a spherical-shoulder approximation. Precise solutions are determined using numerical iterations initialized with the approximate solutions. The method is exhaustive and efficient, thus providing a tool for optimization of grasp strategies.

Given the harsh kinematic constraints, additional degrees of freedom must be introduced to realize solutions. For horizontal grasp solutions, our strategy is to plan the robot's approach, such that a desired grasp pose is within the pre-computed reachable space of the robot. For valve turning and door-handle manipulation, we use non-prehensile manipulation, thus reducing the dimensionality of the target poses. In many instances, constraining the palm normal direction and the palm-frame origin—providing a 1-DOF null space—is sufficient to offer a continuum of solutions. Choosing a specific task trajectory from among the options can be performed by specifying additional metrics, such as torque sensitivity, manipulability, approachability, and trajectory smoothness.

#### REFERENCES

- [1] <http://www.theroboticschallenge.org>
- [2] [http://www.bostondynamics.com/robot\\_Atlas.html](http://www.bostondynamics.com/robot_Atlas.html)
- [3] M. Quigley, C. Salisbury, A. Ng, J.K. Salisbury, "Mechatronic Design of an integrated Robotic Hand", Int J. Robotics Research, Feb, 2014.
- [4] [http://wiki.ros.org/Industrial/Tutorials/Create\\_a\\_Fast\\_IK\\_Solution](http://wiki.ros.org/Industrial/Tutorials/Create_a_Fast_IK_Solution)
- [5] Denavit, J.; Hartenberg, R. S. (1955). "A kinematic notation for lower-pair mechanisms based on matrices". *Trans ASME J. Appl. Mech* 23: 215–221.
- [6] Lorenzo Sciavicco, Bruno Siciliano, *Modelling and Control of Robot Manipulators*. Springer-Verlag, London, 2000, pp. 70–75.
- [7] Pieper, D.L., “The Kinematics of Manipulators Under Computer Control”, Ph.D Thesis, Department of Computer Science, Stanford University, 1968.
- [8] Paul, Richard (1981). *Robot manipulators: mathematics, programming, and control : the computer control of robot manipulators*. MIT Press, Cambridge, MA. ISBN 978-0-262-16082-7.
- [9] <http://www.ros.org/>
- [10] <http://wiki.ros.org/kdl>
- [11] <http://eigen.tuxfamily.org>
- [12] [http://openrave.org/docs/latest\\_stable/openravepy/databases.kinematic\\_reachability](http://openrave.org/docs/latest_stable/openravepy/databases.kinematic_reachability)
- [13] G. N Vahrenkamp, T Asfour and R Dillmann, "Robot Placement based on Reachability Inversion," in IEEE International Conference on Robotics and Automation (ICRA), May 2013, pp. 1970-1975.
- [14] MR Cutkosky and RD Howe, "Human Grasp Choice and Robotic Grasp Analysis" in ST Venkataraman, T Iberall eds, *Extrous Robot Hands*, Springer-Verlag, 1990, Ch 1, pp 5-31.
- [15] Newman, W. S., and Zhang, Y., "Stable Interaction Control and Coulomb Friction Compensation Using Natural Admittance Control", Journal of Robotic Systems, Vol. 11, No.1, pp. 3 - 11, 1994.
- [16] Carl de Boor, *A Practical Guide to Splines*, Springer-Verlag, New York, 2001, Chapter XIV